analytical chemistry

pubs.acs.org/ac Article

Electrochemiluminescence Imaging at a Single Nanoparticle Scale to Elucidate Diffusion-Accelerated Charge Transfer and Monitor Cell Permeability

Xiangfu Hu, Siqi Yu, Chao Wang, Xiaobo Zhang, Jianbin Pan, and Huangxian Ju*

Cite This: *Anal. Chem.* 2023, 95, 4496−4502 Read Online

ACCESS | Metrics & More | Article Recommendations | Supporting Information

ABSTRACT: Accelerating the charge transfer between electroactive species and the electrode is always a hot topic. Here, we report a finding of $Ru(bpy)_3^{3+}$ diffusion-induced acceleration of charge transfer from $Ru(bpy)_3^{2+}$-doped silica nanoparticles (RDSNs) to the electrode via electrochemiluminescence (ECL) imaging at a single nanoparticle scale. $Ru(bpy)_3^{2+}$ in the electrolyte can act as an enhancer of RDSN ECL emission in the presence of coreactant tripropylamine, which amplifies the RDSN ECL by 478 times at 10 μM free $Ru(bpy)_3^{2+}$. According to percolation theory, the diffusion of electro-generated $Ru(bpy)_3^{3+}$ near a single RDSN brings much quicker charge transfer to the electrode than electron hopping in RDSN, which is demonstrated by spatial and temporal interaction imaging of the RDSN and the Ru(III) diffusion layer. Taking advantage of this new mechanism, a real-time ECL imaging method has been constructed to monitor the rapid change of cell permeability during surfactant treatment.

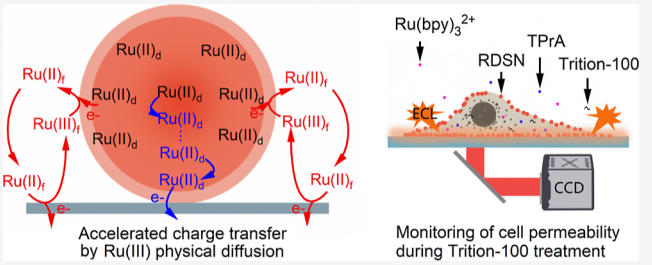

INTRODUCTION

Electrochemiluminescence (ECL) has been widely applied in the detection of trace substances benefiting from its near to zero background.[1,2] The surface-confined luminescence caused by an electro-generated coreactant radical with a short lifetime makes the results of ECL imaging similar to those of total internal reflection fluorescence (TIRF) microscopy with low out-of-focus interference and a high signal-to-noise ratio (SNR), which has been used to probe cell−matrix adhesion[3] and membrane protein imaging.[4,5] However, compared with photoluminescence (PL), the much weaker signal from the ECL process limits its application in micro-imaging, especially in dynamic imaging with high time resolution.

Enriching ECL active molecules into a nanoemitter has been considered as a simple way to enhance the ECL signal.[6] For example, $Ru(bpy)_3^{2+}$-doped silica nanoparticles (RDSNs), a well-known ECL material[7] concentrating large amounts of $Ru(bpy)_3^{2+}$, have successfully been used as single tags for ECL imaging with a high SNR.[8] However, the long-distance charge-transfer mechanism between the internal $Ru(bpy)_3^{2+}$ and the electrode is still unclear. Two assumptions were given to describe this mechanism: (1) $TPrA^{+\bullet}$ and $TPrA^{\bullet}$ are formed on the electrode by electro-oxidation of TPrA and subsequent deprotonation, which diffuse into silica nanopores to reduce the dopant $Ru(bpy)_3^{2+}$ and oxidize $Ru(bpy)_3^{+}$, respectively, to produce $Ru(bpy)_3^{2+*}$ and (2) $Ru(bpy)_3^{2+}$ is directly oxidized through electron hopping and then reduced by $TPrA^{\bullet}$ to produce $Ru(bpy)_3^{2+*}$.[9,10] To eliminate the interference of leaked $Ru(bpy)_3^{2+}$ in interpreting the ECL process, $Ru(bpy)_3^{2+}$ was covalently doped with silica nanoparticles (SNs).[9] However, the widely used RDSN is usually prepared by non-covalent doping; therefore, it is necessary to elucidate the mechanism in the presence of free $Ru(bpy)_3^{2+}$, which has always been ignored in describing its ECL mechanism.[11,12]

With the progress of weak optical signal detection, single-particle[13] or even single-molecule[14] ECL imaging has become possible. These developed micro-imaging approaches can spatially separate different objects to provide far richer information than conventional ECL detection techniques. Here, we made use of ECL imaging to explore the ECL emission of non-covalently doped $Ru(bpy)_3^{2+}$ at a single nanoparticle scale and found that free $Ru(bpy)_3^{2+}$ in the electrolyte could greatly enhance the ECL of RDSN (Figure 1A). Based on the experimental evidence and charge percolation theory,[15] a $Ru(bpy)_3^{3+}$ diffusion-accelerated charge-transfer mechanism was proposed, which led to a real-time ECL imaging technique for probing the dynamic change of cell permeability.

Received: November 23, 2022
Accepted: February 14, 2023
Published: February 23, 2023

https://doi.org/10.1021/acs.analchem.2c05250
Anal. Chem. 2023, 95, 4496−4502

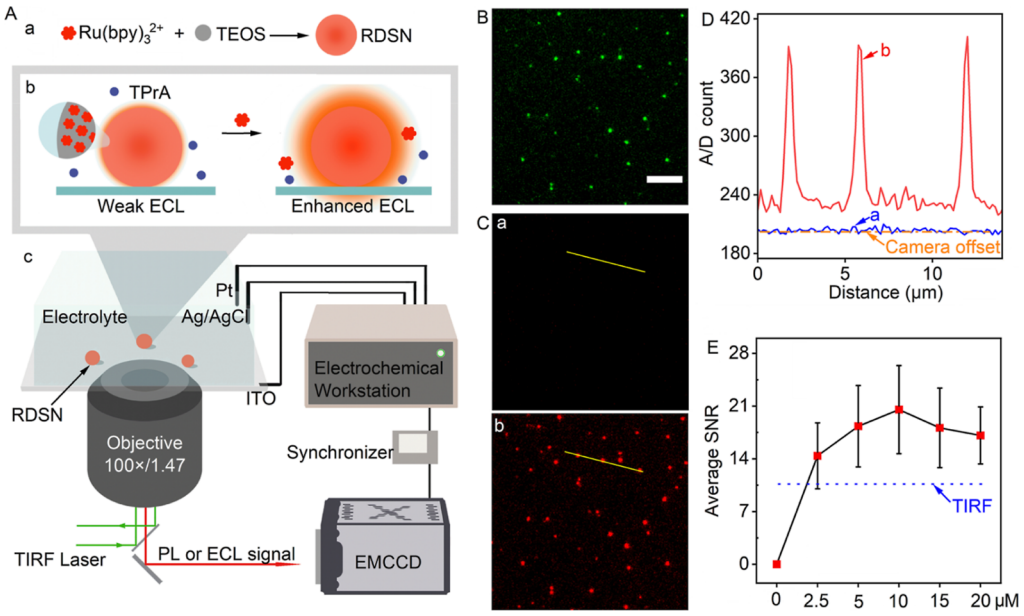

Figure 1. (A) Schematic of (a) synthesis, (b) enhanced ECL, and (c) micro-imaging system of RDSN. (B) TIRF image of RDSN. (C) ECL images of RDSN in the presence of 10 mM TPrA (a) and 10 μM $Ru(bpy)_3^{2+}$ (b). (D) ECL intensity profiles cross yellow lines in (C). (E) Average SNR of ECL spots at different concentrations of $Ru(bpy)_3^{2+}$ at 1.4 V with an exposure time of 15 s. Scale bar: 5 μm.

EXPERIMENTAL SECTION

Materials and Reagents. The detailed information is described in the Supporting Information (SI).

Synthesis of RDSN. A reverse microemulsion method[16] was used for the synthesis of RDSN. The oil phase consisted of 7.5 mL of cyclohexane and 1.8 mL of *n*-hexanol. After 340 μL of 50 mM $Ru(bpy)_3^{2+}$ and 1.77 mL of Triton X-100 surfactant were added to the oil phase and stirred for 30 min, the mixture became limpid due to the formation of a reverse microemulsion. Next, 100 μL of tetraethyl orthosilicate and 60 μL of NH_3H_2O were added to the microemulsion solution under stirring to initiate the reaction at 25 °C for 24 h. To collect the RDSN nanoparticles, 8 mL of acetone was added to the reaction mixture to break the microemulsion, and the precipitate was centrifuged and washed with 10 mL of ethanol and water. Surface-functionalized RDSNs, RDSN-COOH and RDSN-NH_2, were obtained by adding 40 μL of (3-aminopropyl)triethoxysilane and carboxyethylsilanetriol sodium salt (CTES) to the reaction mixture for 6 h, respectively, and the precipitate was centrifuged and washed with 10 mL of ethanol and water. All RDSN products were freeze-dried and stored at 4 °C.

Preparation of Cy3@SNs, RDSN@Silica Microball, WGA@RDSN Nanoprobe, and PAA@RDSN. The synthesis and carboxylation of SNs were performed with the same method described above except for replacing $Ru(bpy)_3^{2+}$ solution with water. Cyanine3 (Cy3)@SNs, the wheat germ agglutinin (WGA) @RDSN nanoprobe, and the RDSN@silica microball were synthesized by the amidation reaction. First, 3 μL of 40 mg/mL SN-COOH or RDSN-COOH was added to 125 μL of NHS (20 mg/mL in 2.5 × morpholineethanesulfonic (MES), pH 5.0). Then, 125 μL of freshly prepared EDC solution (20 mg/mL in 2.5 × MES, pH 5.0) was added to activate the carboxyl group on nanoparticles for 30 min at room temperature. The obtained nanoparticles were centrifuged and washed with 1 mL of water at 4 °C twice to remove excess dehydrating agent and then dispersed in 500 μL of cold 10 mM pH 7.4 phosphate-buffered saline (PBS). Afterward, 20 μL of 500 nM Cy3-DNA linker-NH_2 or 2 mg/mL WGA (in 10 mM PBS, pH7.4) or 2.5 μL of aminodized silica microball (2.5 wt %, in water) was added, respectively. After reaction for 3 h at room temperature, the obtained Cy3@SNs, WGA@RDSN, and RDSN@silica microball were each centrifuged and washed with 1 mL of water three times. These products were dispersed in 500 μL of water and stored at 4 °C.

Polyacrylic acid (PAA) @RDSN was synthesized by an electrostatic adsorption method.[16] 0.5 mg of RDSN-COOH was mixed with 1 mL of poly dimethyl diallyl ammonium chloride (PDDA) (1 mg/mL) under vigorous stirring for 30 min and centrifuged and washed with water twice. After the obtained PDDA@RDSN was dispersed in 1 mL of PAA (2 mg/mL) for 30 min, the product PAA@PDDA@RDSN (PAA@RDSN) was centrifuged and cleaned with water.

TIRF and ECL Imaging of Nanoparticles. The PL and electrochemiluminescence (ECL) images of RDSN were taken by a TIRF microscope (DMI8-TIRF AM, Leica, Germany) equipped with an ultrasensitive EMCCD (ixon Ultra 897u, Andor, UK) at single photon sensitivity operated by ANDOR SOLIS software and cooling to −95 °C. Photons emitted from nanoparticles were collected by an oil immersion objective with high numerical aperture (HCX PL APO 100×/1.47).

For TIRF imaging, a 488 nm laser was used as a fluorescence excitation source. The fluorescence filter box consisted of a 500 nm dichroic mirror and a 520 nm high-pass EM filter which was fit to the $Ru(bpy)_3^{2+}$ wide fluorescent or ECL emission.

The ECL signal was excited by a three-electrode electrochemical workstation (CHI660D, Chenhua Co., Ltd, China) with a homemade indium tin oxide (ITO) slip as the working electrode (WE), a Pt wire as the counter electrode, and Ag/AgCl as the reference electrode. The camera exposure was triggered by the electrochemical workstation output signal from the serial interface through a homemade digital simultaneous device, which could also record the return signal from the camera during the exposure.

https://doi.org/10.1021/acs.analchem.2c05250
Anal. Chem. 2023, 95, 4496−4502

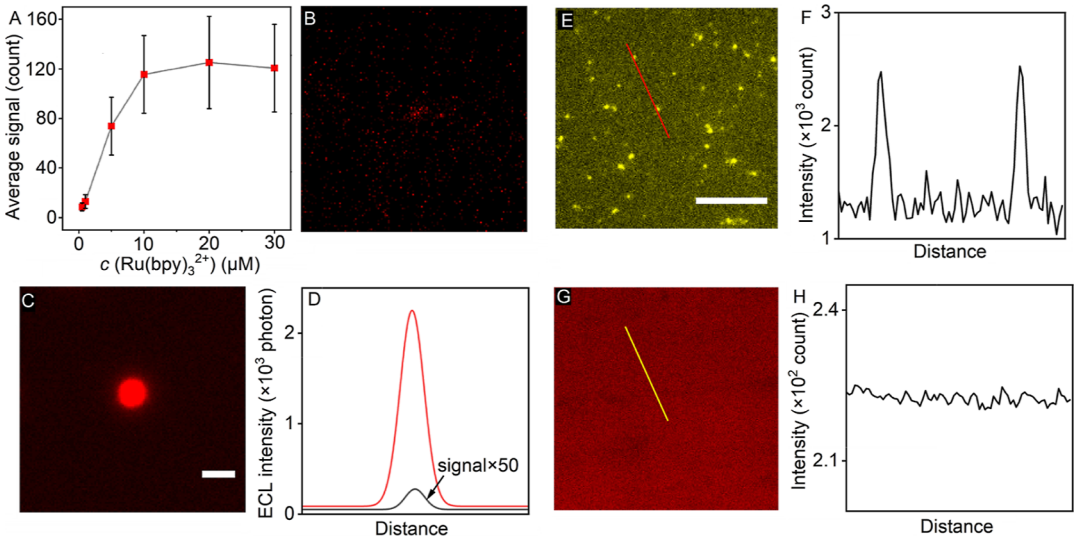

Figure 2. (A) Effect of $Ru(bpy)_3^{2+}$ concentration on the ECL signal of RDSN spots in the presence of 10 mM TPrA at 1.4 V and exposure time of 15 s. (B, C) ECL images of same RDSN@silica microball in 0.1 M PBS (pH 7.4) containing 0.1 M KNO_3, 10 mM TPrA, and (B) 0 and (C) 10 μM $Ru(bpy)_3^{2+}$ at 1.4 V and exposure time of 15 s. (D) ECL signal profiles of RDSN@silica microball in B (black) and C (red). Scale bar: 5 μm. (E) TIRF image and (F) intensity profile of Cy3@SNs. Scale bar: 10 μm. (G) ECL image and (H) ECL intensity profile of Cy3@SNs in 0.1 M PBS (pH 7.4) containing 0.1 M KNO_3, 10 mM TPrA, and 10 μM $Ru(bpy)_3^{2+}$ at 1.4 V and exposure time of 15 s.

Culture and Fixing of HeLa Cells in the Electrolytic Cell. HeLa cells from Cell Bank of Chinese Academy of Sciences (Shanghai, China) were cultured in high glucose Dulbecco's modified Eagle's medium (DMEM) added with 10% fetal bovine serum and 1% penicillin streptomycin on a 40 mm diameter culture dish at 37 °C with 5% CO_2 in a constant humidity incubator. When adherent cells reached the exponential growth phase, the culture dish was washed with 2 mL of 1× PBS three times to remove the glucose in medium. 2 mL of 1× PBS containing 20 μL of WGA@RDSN was then added into the dish to incubate for 10 min at room temperature. Afterward, the dish was washed with 2 mL of 1× PBS three times, and cells were digested with 1 mL of trypsin (0.1%, m/v) for 40 s, which was stopped by adding 3 mL of culture medium. After centrifuging, the WGA@RDSN-labeled living cells were suspended in 1 mL of DMEM and then seeded in the electrolytic cell for 6 h. Finally, the adherent cells on ITO were fixed with 60 μL of paraformaldehyde (4%) for 10 min at 4 °C.

Real-Time ECL Imaging of Cell Permeability. 60 μL of PBS (0.01 M, pH 7.4) containing 10 μM $Ru(bpy)_3^{2+}$ and 10 mM TPrA was dropped in the fixed electrolytic cell to continuously record the series of ECL images with a camera in the photon counting model under applying potential pulses of 1.4 V with 1 s intervals. After 20 s, the electrolyte was quickly replaced with 60 μL of PBS (0.01 M, pH 7.4) containing 0.1% Triton X-100, 10 μM $Ru(bpy)_3^{2+}$, and 10 mM TPrA to continuously record the ECL images for 360 s.

RESULTS AND DISCUSSION

Characterization and ECL Imaging of RDSN. The transmission electron microscopic images of RDSN revealed a spheroid with an average size of 50 nm (Figure S1). A single RDSN was estimated to contain about 26 000 $Ru(bpy)_3^{2+}$. These nanoparticles could be coated on a super-thin ITO WE to show spatially separated fluorescenct spots at the single particle scale under the TIRF laser excitation (Figures 1B and S2A,B). In the presence of TPrA and free $Ru(bpy)_3^{2+}$, the single RDSN showed bright ECL spots at the positions of the TIRF spots, while the ECL signal was unobservable in the absence of free $Ru(bpy)_3^{2+}$ (Figure 1C), which was below the single-photon level as the background, even at a high TPrA concentration and the maximum camera sensitivity (Figures 1D and S2C–J), though the ECL signal of RDSN coating could be detected with a photomultiplier tube (Figure S3), indicating the enhancement of free $Ru(bpy)_3^{2+}$ on ECL emission of RDSN.

The SNR and intensity of ECL spots increased with increasing $Ru(bpy)_3^{2+}$ concentration in the electrolyte and reached the maximum value at 10 μM (Figures 1E and 2A). To estimate the effect of free $Ru(bpy)_3^{2+}$ on ECL emission of RDSN, the RDSN-coated silica microball was synthesized to be immobilized on the ITO electrode, which showed a signal at 10 μM $Ru(bpy)_3^{2+}$ that is about 478 times more than that of the signal observed in the absence of free $Ru(bpy)_3^{2+}$ (Figure 2B–D). Both the silica microball and Cy3@SNs modified electrodes did not produce observable ECL signal at 10 μM $Ru(bpy)_3^{2+}$ (Figures 2E–H and S4), indicating that the dopant $Ru(bpy)_3^{2+}$ was also crucial to the formation of ECL spots. Moreover, the background ECL emitted from homogeneous $Ru(bpy)_3^{2+}$/TPrA on RDSN was negligible (Figure S5), revealing that free $Ru(bpy)_3^{2+}$ enhanced the ECL of dopant $Ru(bpy)_3^{2+}$ by 478 times.

Oxidation of $Ru(bpy)_3^{2+}$ in RDSN. We applied the concept of operando ECL imaging[17] to study the ECL frequency (f_{ECL}) change of RDSN in $Ru(bpy)_3^{2+}$/TPrA upon potential scanning at a single nanoparticle scale (Figure S6). The f_{ECL} was calculated by photon counting (inset in Figure 3A), and the f_{ECL}–potential curve exhibited a strong ECL peak at +1.4 V (Figure 3A), which was different from mechanism (1) at around +1.0 V, the "low oxidation potential" route (Figure S3),[9] but similar to mechanism (2), the "oxidation–reduction" route and was also demonstrated to be related to the direct oxidation of local $Ru(bpy)_3^{2+}$ (Figure S7). However, the dependence of ECL signal on the TPrA concentration (Figure 3B) was different from the proportional relationship

https://doi.org/10.1021/acs.analchem.2c05250
Anal. Chem. 2023, 95, 4496–4502

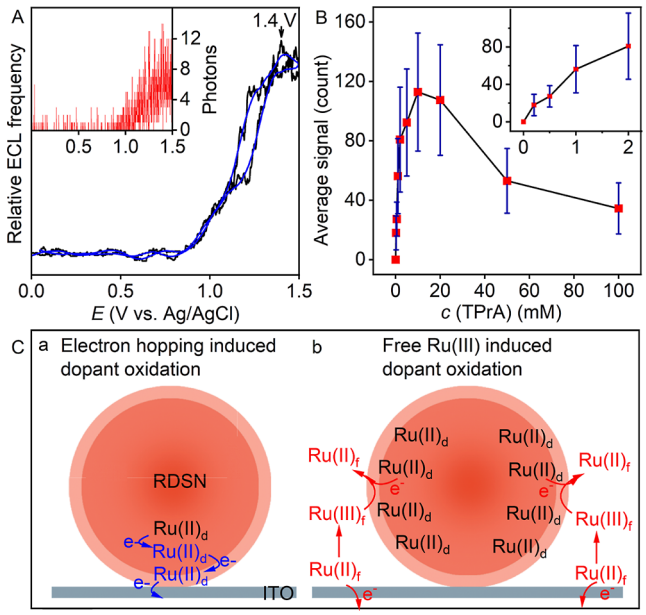

Figure 3. (A) RDSN ECL frequency−potential curve (black) and its smoothing curve (blue) in the presence of 10 mM TPrA and 10 μM $Ru(bpy)_3^{2+}$ at 0.1 V/s. Inset: background deducted photon signal of RDSN at 20 pixels. (B) Effect of TPrA concentration on the ECL signal of RDSN in the presence of 10 μM $Ru(bpy)_3^{2+}$ at 1.4 V and exposure time of 15 s. Inset: low concentration range. (C) Schematic of (a) electron hopping and (b) free Ru(III)-induced internal $Ru(bpy)_3^{2+}$ oxidation. Subscripts f and d denote free and dopant, respectively.

observed for the general $Ru(bpy)_3^{2+}$/TPrA system at the "oxidative-reduction" route,[18] implying a different ECL mechanism.

According to mechanism (2), the direct oxidation of dopant $Ru(bpy)_3^{2+}$ in RDSN at high potential contributed to the electron hopping, as shown in Figure 3C(a). However, the typical distance of electron hopping was only ~1−2 nm from the electrode,[9] which was difficult to trigger enough dopant $Ru(bpy)_3^{2+}$ oxidation for producing an observable ECL signal at the single nanoparticle scale. When the electrolyte contains free $Ru(bpy)_3^{2+}$, the electro-generated Ru(III) could diffuse into RDSN to oxidize the dopant $Ru(bpy)_3^{2+}$ [Figure 3C(b)], which brought an additional charge-transfer pathway from the electrode to RDSN and thus produce much stronger ECL emission. To better understand the effect of free $Ru(bpy)_3^{2+}$ on charge transfer between the dopant $Ru(bpy)_3^{2+}$ and the electrode, we used charge percolation theory to quantify two processes in terms of charge transport diffusion coefficient, D_{CT}.[19−21]

When charge transfer is caused by the physical diffusion of charged ions, the transport can be approximated as a mean-field behavior,[15] and the coefficient can be written as

$$D_{CT} = D_P \quad (1)$$

where D_P denotes the physical diffusion coefficient and is equal to 5×10^{-6} cm^2 s^{-1} for most substances in aqueous solution.

The D_{CT} of electron hopping in RDSN can be estimated by the Fritsch-Faules−Faulkner model (details are presented in the Supporting Information)[22,23]

$$D_{CT} = D_E = \frac{1}{6} A \langle r_{nn}^2 \rangle \exp\left(\frac{r_0 - \langle r_{nn} \rangle}{k}\right) \quad (2)$$

where D_E denotes the electron hopping coefficient, A is the pre-exponential factor, k is the characteristic distance describing the spatial extant of electronic coupling in the medium, r_{nn} is the average nearest-neighbor separation, and r_0 is the contact radius.[22] In RDSN, the value of D_E was calculated to be about 8.5×10^{-9} cm^2 s^{-1}. Although different models have been used,[24] the obtained D_E are of the same order of magnitude.[25,26] Thus, the D_{CT} in RDSN was much lower than the physical diffusion coefficient, leading to the oxidation of less $Ru(bpy)_3^{2+}$ by hopping.[27] In this regard, the diffusion of electro-generated $Ru(bpy)_3^{3+}$ accelerated the charge transfer between the RDSN and the electrode.

The electron hopping in RDSN led to a low $Ru(bpy)_3^{3+}$ concentration on the surface of RDSN. From the Nernst equation, the potential of $Ru(bpy)_3^{3+}/Ru(bpy)_3^{2+}$ on the surface of RDSN is lower than that of the free $Ru(bpy)_3^{3+}/Ru(bpy)_3^{2+}$ on the solution/RDSN interface due to the quick physical diffusion of free $Ru(bpy)_3^{3+}$, which drove the electron exchange between $Ru(bpy)_3^{2+}$ in the RDSN surface and free $Ru(bpy)_3^{3+}$ in the solution/electrode interface for the oxidation of $Ru(bpy)_3^{2+}$ inside the silica nanosphere by $Ru(bpy)_3^{3+}$ from the free solution.

Interaction Imaging of RDSN and $Ru(bpy)_3^{3+}$ Diffusion Layer. Spatial and temporal ECL imaging was designed to demonstrate the interaction between RDSN and electro-generated $Ru(bpy)_3^{3+}$ in the diffusion layer. The spatial ECL imaging was performed with the RDSN@silica microball, on which most RDSNs moved away from the electrode, and their oxidation completely depended on the contact with $Ru(bpy)_3^{3+}$ and the diffusion layer thickness of $Ru(bpy)_3^{3+}$ [Figure 4A,B(a)].[28−31] At high $Ru(bpy)_3^{2+}$ concentration,s the size of ECL spots was close to the diameter of he tmicroball, while it was much smaller at low $Ru(bpy)_3^{2+}$ concentrations [Figure 4A,B(b,c)], indicating that only the RDSN contacting with $Ru(bpy)_3^{3+}$ could be lit up to produce enhanced ECL emission. Moreover, the temporal ECL imaging of RDSN in $Ru(bpy)_3^{2+}$/TPrA (Figure 4C) showed high synchronization between the electro-oxidation of $Ru(bpy)_3^{2+}$ at 7.93 to 8.04 s [Figure 4D(a)] and the background-deducted ECL emission of RDSN (7.95 to 8.05) [Figure 4D(b)], demonstrating that the ECL signal resulted from the formation of $Ru(bpy)_3^{3+}$.

Diffusion-Accelerated Charge-Transfer Mechanism of RDSN. From the above discussion, we could propose a $Ru(bpy)_3^{3+}$ diffusion-accelerated charge-transfer mechanism to describe the greatly enhanced ECL of RDSN. In the presence of free $Ru(bpy)_3^{2+}$, electro-generated $Ru(bpy)_3^{3+}$ acted as a charge carrier to deliver charge from the electrode to the dopant $Ru(bpy)_3^{2+}$ in RDSN by its physical diffusion. This process led to the oxidation of dopant $Ru(bpy)_3^{2+}$ and was much quicker than electron hoping in RDSN. Subsequently, the formed dopant $Ru(bpy)_3^{3+}$ reacted with $TPrA^{\bullet}$ to emit the ECL (Figure 5A(a)). The ceaseless turnover of Ru(II)/Ru(III) near the single RDSN ensured sufficient electron flux from the RDSN to the electrode, which led to a high local turnover frequency (TOF) to eventually enhance the RDSN ECL signal [Figure 5A(b)]. Undeniably, the electro-generated $TPrA^{\bullet}$ could quench the electro-generated $Ru(bpy)_3^{3+}$ in the electrolyte to produce the ECL background (TOF_1), which led to a decreased ECL intensity of RDSN spots at a high TPrA concentration (Figure 2B). The effect of excess coreactant on the ECL signal was further verified by replacing TPrA with 2-(dibutylamino)ethanol (DBAE), a coreactant with higher activity,[32] which showed a much lower ECL signal

https://doi.org/10.1021/acs.analchem.2c05250
Anal. Chem. 2023, 95, 4496−4502

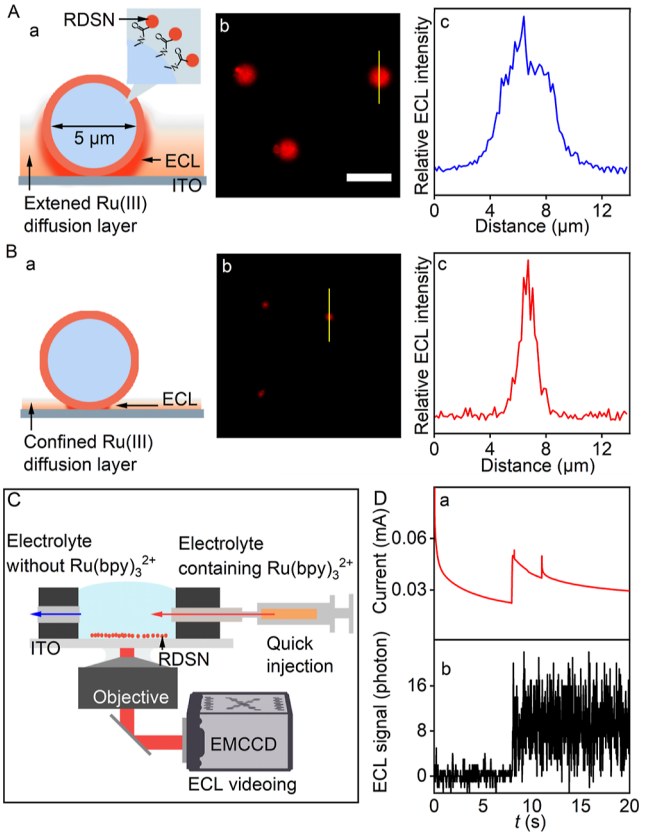

Figure 4. (A,B) (a) Schematic of ECL imaging of interaction of RDSN and Ru(III) diffusion layer on spatial, (b) ECL image, and (c) intensity profile of RDSN@silica microball in the presence of 1 mM TPrA and 10 μM (A) or 100 nM (B) $Ru(bpy)_3^{2+}$ at 1.4 V. Exposure time = 15 s. Scale bar: 10 μm. (C) Schematic of ECL videoing of interaction of RDSN and Ru(III) diffusion layer on temporal. When the electrolyte without $Ru(bpy)_3^{2+}$ is rapidly replaced with the electrolyte containing 10 μM $Ru(bpy)_3^{2+}$, the electrochemical and ECL signals of single RDSN on ITO at 1.4 V is recorded simultaneously. (D) Synchronizing current (a) and background-deducted ECL (b) signals recorded from (C). Electrolyte: 0.1 M PBS (pH 7.4) containing 0.1 M KNO_3 and 10 mM TPrA. Exposure time: 10 ms. Frame rate: 96 s^{-1}.

of RDSN (Figure 5B), contrary to the stronger ECL of $Ru(bpy)_3^{2+}$/DBAE in solution.[29] Similarly, the ECL signal of RDSN decreased greatly after covering it with polymer coating to prevent its contact with external $Ru(bpy)_3^{3+}$ (Figure 5C).

Real-Time ECL Imaging to Monitor Cell Permeability during Surfactant Treatment. The ECL emission of RDSN/TPrA in the presence of free $Ru(bpy)_3^{2+}$ kept the signal confinement feature of the ECL nanoemitter and could meet the needs of dynamic ECL imaging at a single tag scale. Through designing a signal switch, the RDSN could be used as a sensitive reporter for monitoring the change of local $Ru(bpy)_3^{2+}$ concentration. Herein, a real-time ECL videoing method was proposed to study the rapid change of cell permeability during surfactant-induced cell permeabilization treatment.[8,33] Using the surfactant Triton X-100 as the cell permeating reagent,[8,33] the electrolyte containing Triton X-100 could pass through cells to light up the RDSN labeled on cells (Figure 6A). The real-time ECL images showed rapid generation of the ECL spots (Figure 6B), which were not observed outside the cell or in the absence of Triton X-100 (Figure S8). The low ECL background of RDSN-labeled HeLa

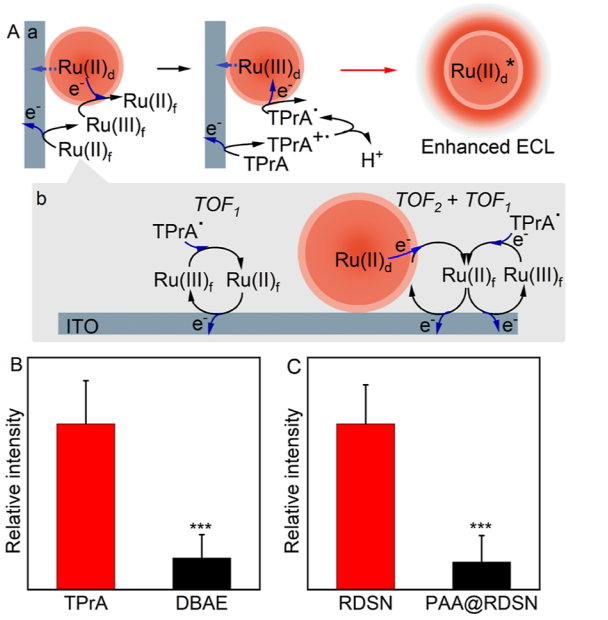

Figure 5. (A) Schematic of (a) ECL emission of RDSN by Ru(III) diffusion-induced dopant oxidation and (b) local electrode process. TOF: turnover frequency. Effects of (B) 10 mM coreactant in 0.1 M (pH 7.4) PBS containing 0.1 M KNO_3 and 10 μM $Ru(bpy)_3^{2+}$ upon scanning from 0 to 1.4 V (0.1 V/s), and (C) surface polymer coating in 0.1 M PBS (pH 7.4) containing 0.1 M KNO_3, 10 μM $Ru(bpy)_3^{2+}$, and 10 mM TPrA at 1.4 V. Exposure time = 15 s.

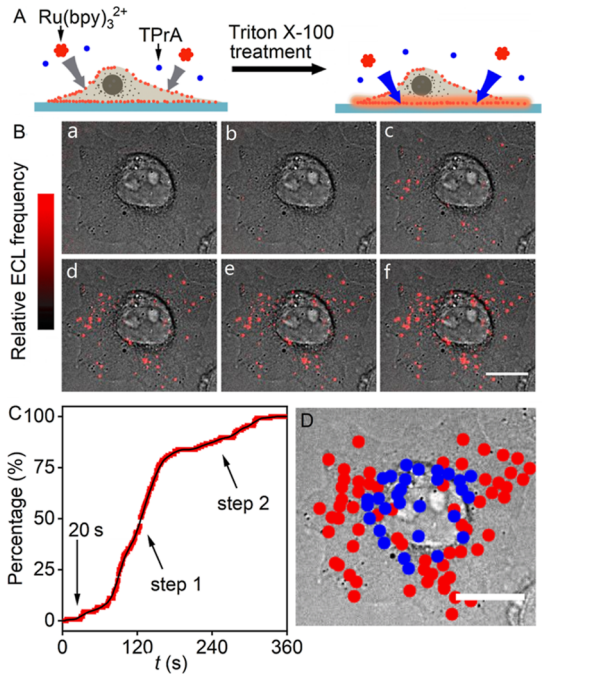

Figure 6. (A) Schematic of real-time ECL imaging of cell permeability. (B) Merged bright field and ECL images of WGA@RDSN-labeled HeLa cells in 0.1 M PBS (pH 7.4) containing 0.1 M KNO_3, 10 mM TPrA, and 10 μM $Ru(bpy)_3^{2+}$ after applying 1.4 V pulses with 1 s interval for 20, 40, 60, 80, 140, and 260 s (a–f), during which the electrolyte was replaced with that containing 0.1% Triton X-100 at 20 s. (C) Percentage of spots reaching the maximum ECL frequency. (D) Spots in steps 1 (red) and 2 (blue) in (C). Scale bar: 15 μm.

https://doi.org/10.1021/acs.analchem.2c05250
Anal. Chem. 2023, 95, 4496−4502

cells (Figure S9) resulted in the possibility to kinetically analyze the cell permeabilization process in different cell areas (Figure S10) and/or to distinguish the endocytosis of RDSN into subcellular organelles at a single probe spot scale. After the cells were treated for 130 s, the number of ECL spots with the maximum ECL frequency reached 81% of the maximum lighted RDSN number, which was achieved at 310 s, indicating complete cell permeabilization (Figure 6C). Interestingly, the obvious difference in the increasing rate of ECL spots occurred at different cell regions (Figure 6D), such as the cell nucleus (blue) and cytoplasm (red) regions. The cell nucleus showed the slowest increase of ECL spots, suggesting the hindrance of the cell nucleus to the diffusion of electroactive species. Thus, the cell permeabilization could be divided into two steps: quick cytoplasm permeabilization in about 2 min and slow nucleus permeabilization in about 5 min. This result provided useful information for reducing possible cell damage in related research.

CONCLUSIONS

A $Ru(bpy)_3^{3+}$ diffusion-accelerated charge-transfer mechanism has been proposed to elucidate the enhancement of RDSN ECL, a phenomenon that is always ignored. The diffusion of electro-generated $Ru(bpy)_3^{3+}$ in an electrolyte to a single RDSN can bring much quicker charge transfer than electron hopping in RDSN to oxidize the dopant $Ru(bpy)_3^{2+}$ and then emit ECL via the reduction of the electro-generated coreactant radical. This leads to an ECL intensity that is amplified by 478 times at 10 μM free $Ru(bpy)_3^{2+}$ and achieves sensitive ECL imaging at a single nanoparticle scale. Taking advantage of this mechanism, a real-time ECL imaging method has been designed to probe the surfactant-induced cell permeabilization process. This work provides an in-depth understanding of charge transfer between the electrode and the $Ru(bpy)_3^{2+}$-doped ECL nano-emitter and shows great potential in digital ECL analysis and ECL nano-imaging.

ASSOCIATED CONTENT

Supporting Information

The Supporting Information is available free of charge at https://pubs.acs.org/doi/10.1021/acs.analchem.2c05250.

Chemicals and reagents, homemade ITO slips and electrolytic cell,estimation of $Ru(bpy)_3^{2+}$ number in single RDSN, brief discussion of percolation theory, data analysis, TEM images, TIRF and ECL images, ECL and CV curves, ECL images, schematic of dynamic ECL imaging, potential optimization for ECL emission, effect of applying potential on the ECL image of control HeLa cells, and kinetic analysis of ECL frequency (PDF)

AUTHOR INFORMATION

Corresponding Author

Huangxian Ju − *State Key Laboratory of Analytical Chemistry for Life Science, School of Chemistry and Chemical Engineering, Nanjing University, Nanjing 210023, P.R. China;* orcid.org/0000-0002-6741-5302; Phone: +86-25-89683593; Email: hxju@nju.edu.cn

Authors

Xiangfu Hu − *State Key Laboratory of Analytical Chemistry for Life Science, School of Chemistry and Chemical Engineering, Nanjing University, Nanjing 210023, P.R. China*

Siqi Yu − *State Key Laboratory of Analytical Chemistry for Life Science, School of Chemistry and Chemical Engineering, Nanjing University, Nanjing 210023, P.R. China*

Chao Wang − *State Key Laboratory of Analytical Chemistry for Life Science, School of Chemistry and Chemical Engineering, Nanjing University, Nanjing 210023, P.R. China*

Xiaobo Zhang − *State Key Laboratory of Analytical Chemistry for Life Science, School of Chemistry and Chemical Engineering, Nanjing University, Nanjing 210023, P.R. China;* orcid.org/0000-0003-0222-2515

Jianbin Pan − *State Key Laboratory of Analytical Chemistry for Life Science, School of Chemistry and Chemical Engineering, Nanjing University, Nanjing 210023, P.R. China*

Complete contact information is available at: https://pubs.acs.org/10.1021/acs.analchem.2c05250

Notes

The authors declare no competing financial interest.

ACKNOWLEDGMENTS

The authors acknowledge the financial support of the National Natural Science Foundation of China (21890741 and 21827812).

REFERENCES

(1) Zhang, J.; Arbault, S.; Sojic, N.; Jiang, D. *Annu. Rev. Anal. Chem.* **2019**, *12*, 275−295.

(2) Ma, C.; Cao, Y.; Gou, X.; Zhu, J. *Anal. Chem.* **2020**, *92*, 431−454.

(3) Ding, H.; Guo, W.; Su, B. *Angew. Chem., Int. Ed.* **2020**, *59*, 449−456.

(4) Wang, N.; Gao, H.; Li, Y.; Li, G.; Chen, W.; Jin, Z.; Lei, J.; Wei, Q.; Ju, H. *Angew. Chem., Int. Ed.* **2021**, *60*, 197−201.

(5) Valenti, G.; Scarabino, S.; Goudeau, B.; Lesch, A.; Jović, M.; Villani, E.; Sentic, M.; Rapino, S.; Arbault, S.; Paolucci, F.; Sojic, N. *J. Am. Chem. Soc.* **2017**, *139*, 16830−16837.

(6) Zhang, L.; Dong, S. *Anal. Chem.* **2006**, *78*, 5119−5123.

(7) Zanut, A.; Palomba, F.; Rossi Scota, S. M.; Rebeccani, S.; Marcaccio, M.; Genovese, D. A.; Rampazzo, E. X.; Valenti, G.; Paolucci, F.; Prodi, L. *Angew. Chem., Int. Ed.* **2020**, *59*, 21858−21863.

(8) Liu, Y.; Zhang, H.; Li, B.; Liu, J.; Jiang, D.; Liu, B.; Sojic, N. *J. Am. Chem. Soc.* **2021**, *143*, 17910−17914.

(9) Zanarini, S.; Rampazzo, E.; Ciana, L. D.; Marcaccio, L. d.; Marzocchi, M.; Montalti, M.; Paolucci, E.; Prodi, E.; Montalti, M.; Montalti, M.; Paolucci, F.; Paolucci, F. l.; Prodi, L. *J. Am. Chem. Soc.* **2009**, *131*, 2260−2267.

(10) Miao, W.; Choi, J. P.; Bard, A. J. *J. Am. Chem. Soc.* **2002**, *124*, 14478−14485.

(11) Ma, C.; Wu, W.; Li, L.; Wu, S.; Zhang, J.; Chen, Z.; Zhu, J. J. *Chem. Sci.* **2018**, *9*, 6167−6175.

(12) Li, B.; Huang, X.; Lu, Y.; Fan, Z.; Li, B.; Jiang, D.; Sojic, N.; Liu, B. *Adv. Sci.* **2022**, *9*, 2204715.

(13) Zhu, M. J.; Pan, J. B.; Wu, Z. Q.; Gao, X. Y.; Zhao, W.; Xia, X. H.; Xu, J.; Chen, H. Y. *Angew. Chem., Int. Ed.* **2018**, *57*, 4010−4014.

(14) Dong, J.; Lu, Y.; Xu, Y.; Chen, F.; Yang, J.; Chen, Y.; Feng, J. *Nature* **2021**, *596*, 244−249.

(15) Blauch, D. N.; Saveant, J. M. *J. Am. Chem. Soc.* **1992**, *114*, 3323−3332.

(16) Sardesai, N.; Barron, J. C.; Rusling, J. F. *Anal. Chem.* **2011**, *83*, 6698−6703.

(17) Dong, J.; Xu, Y.; Zhang, Z.; Feng, J. *Angew. Chem., Int. Ed.* **2022**, *61*, No. e202200187.

(18) Miao, W. *Chem. Rev.* **2008**, *108*, 2506−2553.
(19) Murray, R. W. *Acc. Chem. Res.* **1980**, *13*, 135−141.
(20) Lyons, M. E. G. *Analyst* **1994**, *119*, 805−826.
(21) Botár, L.; Ruff, I. *Chem. Phys. Lett.* **1986**, *126*, 348−351.
(22) Fritsch-Faules, I.; Faulkner, L. R. *J. Electroanal. Chem.* **1989**, *263*, 237−255.
(23) Faulkner, L. R. *Electrochemi. Acta* **1989**, *34*, 1699−1706.
(24) He, P.; Chen, X. *J. Electroanal. Chem.* **1988**, *256*, 353−360.
(25) Majda, M.; Faulkner, L. R. *J. Electroanal. Chem.* **1984**, *169*, 77−95.
(26) Majda, M.; Faulkner, L. R. *J. Electroanal. Chem.* **1984**, *169*, 97−112.
(27) Lv, X.; Li, M.; Guo, Z.; Zheng, X. *Luminescence* **2019**, *34*, 334−340.
(28) Ding, J.; Zhou, P.; Guo, W.; Su, B. *Front. Chem.* **2021**, *8*, 630246.
(29) Guo, W.; Zhou, P.; Sun, L.; Ding, H.; Su, B. *Angew. Chem., Int. Ed.* **2021**, *60*, 2089−2093.
(30) Ma, Y.; Colin, C.; Descamps, J.; Arbault, S.; Sojic, N. *Angew. Chem., Int. Ed.* **2021**, *60*, 18742−18749.
(31) Ding, H.; Zhou, P.; Fu, W.; Ding, L.; Guo, W.; Su, B. *Angew. Chem., Int. Ed.* **2021**, *60*, 11769−11773.
(32) Liu, X. Q.; Shi, L. H.; Niu, W. X.; Li, H. J.; Xu, G. B. *Angew. Chem., Int. Ed.* **2007**, *46*, 421−424.
(33) Voci, S.; Goudeau, B.; Valenti, G.; Lesch, A. A.; Jović, M.; Rapino, S.; Paolucci, F.; Arbault, S.; Sojic, N. *J. Am. Chem. Soc.* **2018**, *140*, 14753−14760.

https://doi.org/10.1021/acs.analchem.2c05250
Anal. Chem. 2023, 95, 4496−4502